

# On the parameterization of ice microphysics in a mesoscale $\alpha$ weather forecast model

N. Mölders<sup>a</sup>, M. Laube<sup>b</sup>, G. Kramm<sup>c</sup>

<sup>a</sup> LIM Institut für Meteorologie, Universität Leipzig, Stephanstr. 3, D-4103 Leipzig, Germany

<sup>b</sup> Universität zu Köln, Institut für Geophysik und Meteorologie, Albertus-Magnus-Platz, D-50923 Köln, Germany

<sup>c</sup> Fraunhofer-Institut für Atmosphärische Umweltforschung (IFU), Kreuzackbahnstraße 19, D-82453 Garmisch-Partenkirchen, Germany

Accepted 25 May 1994

---

## Abstract

Numerical experiments with a 3-D-dimensional mesoscale  $\alpha$  weather forecast model are performed to investigate the sensitivity of the model to different parameters and the parameterized microphysics. The parameterization considers condensation and deposition of water vapor, sublimation, evaporation of both cloud water and rainwater, riming of ice crystals by cloud water, rainwater formation by autoconversion, accretion and melting as well as the sedimentation of rain and ice crystals. The results of the simulations are discussed on the basis of the analysis, estimations of skill and uncertainty, satellite data as well as observed precipitation data. These results show that the dynamics of the troposphere and the cloud microphysics can be described more realistically and that the model performance can be improved if ice processes are included. It is substantiated by all of these simulations that the relative humidity and water substance mixing ratio fields were only strongly altered by turning off the ice phase or the riming process.

---

## 1. Introduction

Results from numerical simulations performed by several authors (e.g., Orville and Kopp, 1977; Cotton et al., 1982; Zhang, 1989; Mölders et al., 1994) show that the additional simulation of ice microphysics in cloud modules results in a better description of cloud and precipitation formation processes. This is due to the fact that the freezing of cloud droplets and the growth of ice crystals by water vapor deposition and riming contribute to latent heat release to enhance cloud growth, to affect the formation of precipitation and to alter the dynamics of cloud fields. Riming, for example, occurs when the terminal velocities of the ice crystals are different from those of supercooled cloud droplets. Furthermore, rain drops

and ice crystals have different shapes, sizes, densities and, hence, terminal velocities. In subsaturated layers rain drops and ice crystals can also evaporate and sublimate, respectively, and, hence, can alter the dynamics of these layers by cooling. These microphysical processes are often not considered in mesoscale  $\alpha$  weather forecast models.

The mesoscale  $\alpha$  forecast model used in this study is the MM4 (Mesoscale Meteorological Model Version 4; Anthes et al., 1987). Usually, it is run with a cumulus parameterization scheme following Kuo (1974) and Anthes (1977). A further parameterization scheme is the warm scheme (Hsie and Anthes, 1984) which treats the microphysics of the warm path of precipitation formation. None of these schemes includes ice processes. But in mid-latitudes and also in tropics the ice phase is an important path for cloud and precipitation formation. Mölders et al. (1994), for example, showed that MM4 running with the warm scheme is overload when strong vertical motions and ice topped clouds are to be simulated. On contrary, running MM4 with the ice parameterization scheme developed by Mölders (1993) (described in Mölders et al., 1994) on the basis of the warm scheme, leads to a more adequate physical and dynamical representation of the simulation of such cloud systems. This ice parameterization mainly follows Cotton et al. (1982). In contrast to the ice parameterization scheme of Dudhia (1989) which has already been utilized in MM4 (Zhang, 1989), in the ice parameterization scheme used in our study ice and supercooled water may coexist within the temperature range from the freezing point to  $-35^{\circ}\text{C}$ .

Several numerical experiments are carried out to investigate the sensitivity of the model to different parameters and the parameterized microphysics. The results of the simulations and their differences to each other are presented and discussed on the basis of the analysis of the NMC (National Meteorological Center) data interpolated from about  $300\text{ km} \times 300\text{ km}$  resolution to the  $80\text{ km} \times 80\text{ km}$  grid mesh used in the model, and NOAA9 AVHRR (Advanced Very High Resolution Radiometer) satellite data. Moreover, the predicted precipitation rates over land are compared with observed data provided by Scheele and Verver (1990). Measures of skill and uncertainty as suggested by Anthes (1983) are determined for further model evaluation. Furthermore, the consequences of the choice of certain parameters are pointed out.

## 2. Parameterization of microphysics

Since MM4 has evolved over the last two decades and has been most thoroughly documented and widely used (e.g., Anthes and Warner, 1978; Anthes et al., 1987) this section describes only the microphysical processes included in the ice parameterization scheme. The condensation and evaporation (denoted as  $\text{CD}_{\text{vc}}$  hereafter), autoconversion ( $\text{CN}_{\text{cr}}$ ), accretion ( $\text{CL}_{\text{cr}}$ ), rainwater evaporation ( $\text{EV}_{\text{rv}}$ ), and the sedimentation of rain are treated like in the warm scheme (Hsie and Anthes, 1984; Anthes et al., 1987).

With respect to the poor horizontal and vertical resolution of mesoscale  $\alpha$  weather forecast models, and because there are generally no observation available to evaluate several predicted ice classes, it seems to be sufficient to include only one ice class covering all from cloud ice to lightly rimed graupel. Thus, the parameterization of ice microphysics includes water vapor deposition and sublimation ( $\text{CD}_{\text{vi}}$ ), cloud water riming onto ice crystals of different sizes ( $\text{CL}_{\text{ci}}$ ), melting ( $\text{ML}_{\text{ir}}$ ), and sedimentation of ice. In the following notation

the subscripts v, c, r, i and s refer to water vapor, cloud water, rainwater, ice particles and saturation, respectively. The parameter  $k$  represents v, c, r, and i. The first subscript denotes the phase being depleted and, the second subscript indicates the water component which is growing. The governing equations for the moisture components  $k$ , the thermodynamic equation and the hydrostatic equation may be written as follows (e.g., Anthes et al., 1987; Mölders et al., 1994)

Moisture budget:

$$\frac{\partial p^* q_k}{\partial t} = -m^2 \left[ \frac{\partial(p^* u q_k/m)}{\partial x} + \frac{\partial(p^* v q_k/m)}{\partial y} \right] - \frac{\partial(p^* q k \dot{\sigma})}{\partial \sigma} + p^* M_k + Dq_k - g \frac{\partial(\rho_a q_k v_{Tk})}{\partial \sigma} \quad (1)$$

with the microphysical processes  $M_k$

$$M_k = \begin{cases} EV_{rv} - CD_{vc} - CD_{vi} & \text{for } k = v \\ CD_{vc} - CN_{cr} - CL_{cr} - CL_{ci} & \text{for } k = c \\ CN_{cr} + CL_{cr} + ML_{ir} - EV_{rv} & \text{for } k = r \\ CD_{vi} + CL_{ci} - ML_{ir} & \text{for } k = i \end{cases}$$

which will be described later in more detail.

Thermodynamic equation:

$$\frac{\partial p^* T}{\partial t} = -m^2 \left[ \frac{\partial(p^* Tu/m)}{\partial x} + \frac{\partial(p^* Tv/m)}{\partial y} \right] - \frac{\partial(p^* T \dot{\sigma})}{\partial \sigma} + \frac{p^* (L_c(CD_{vc} - EV_{rv}) + L_s CD_{vi} + L_f(CL_{ci} - ML_{ir}))}{c_{pm}} + DT + \frac{RT_v \omega}{c_{pm}(\sigma + p_{100}/p^*)} \quad (2)$$

Hydrostatic equation:

$$\frac{\partial \Phi}{\partial \ln(\sigma + p_{100}/p^*)} = -RT_v \left( 1 + \frac{q_c + q_r + q_i}{1 + q_v} \right)^{-1} \quad (3)$$

Here,  $p^*$  is the difference between the pressure at surface,  $p_s$ , and,  $p_{100} = 100$  hPa, the pressure at the top of the model,  $\sigma$  is vertical coordinate of the model,  $u$  and  $v$  are the horizontal components of the wind,  $\dot{\sigma}$  is the vertical velocity,  $m$  is the map scale factor,  $\rho_a$  is the density of the air,  $v_{Tk}$  is the massweighted terminal velocity,  $g$  is the acceleration of gravity,  $q_k$  is the mixing ratio of the phase  $k$ ,  $R$  is the gas constant of dry air, and  $T_v$  is the virtual temperature. Furthermore,  $L_c$ ,  $L_s$ , and  $L_f$  are the latent heat of condensation, sublimation and freezing,  $c_{pm}$  is the specific heat at constant pressure for moist air,  $\omega$  is the vertical velocity in  $p$ -coordinates, and  $DT$  and  $Dq_k$  represent the contributions by diffusion processes (Anthes et al., 1987). It is assumed that in the case of ice and rainwater the effects of vertical diffusion can be neglected in comparison with the contributions by sedimentation. The first three terms on the r.h.s. of Eqs. (1) and (2) represent the transport, and the fourth term describes the changes due to phase transition processes. The last term in Eq. (1) represents the rate of change of phase  $k$  by sedimentation. The fall velocities of cloud

droplets are assumed to be zero. Since only few CCN act as ice nuclei (e.g., Heymsfield and Sabin, 1989) and, hence, the size distributions of ice clouds are spread over few large particles developing quickly fallspeeds of tens of  $\text{cm s}^{-1}$  (e.g., Heymsfield, 1977), cloud ice and settling ice are not distinguished. Thus, fallout is considered immediately after ice has been formed. Assuming a Marshall–Palmer (1948) distribution for the spectral density of precipitation particles and following Srivastava (1967), massweighted mean terminal velocities for rain drops and ice crystals can be written as:

$$v_{Tk} = \frac{a_k \Gamma(4 + b_k)}{6 \lambda_k^{b_k} (\rho_o / \rho_a)^{1/2}}, \quad (4)$$

where  $k$  stands for  $r$  and  $i$ , respectively. Here,  $\Gamma$  is the gamma function,  $(\rho_o / \rho_a)^{1/2}$  is a correction factor to take into account the decreasing of the fall velocity with increasing air density and  $\rho_o$  is the density of a standard atmosphere. The parameters  $a_k$  and  $b_k$  are denoted as  $842 \text{ m}^{1-b_r} \text{ s}^{-1}$  and 0.8 for rainwater (Lui and Orville, 1969), and  $56.4 \text{ m}^{1-b_i} \text{ s}^{-1}$  and 0.57 for ice (Locatelli and Hobbs, 1974), respectively. The size distribution parameters for rain drops and ice particles,  $\lambda_k$ , depend on their respective rainwater and ice mixing ratio, according to

$$\lambda_k = \left( \frac{\pi \rho_k N_{ok}}{\rho_a q_k} \right)^{1/4}, \quad (5)$$

with  $N_{or} = 8 \cdot 10^6 \text{ m}^{-4}$  (Marshall and Palmer, 1948) and  $N_{oi} = 7.6 \cdot 10^6 \text{ m}^{-4}$  (Leary and Houze, 1979). Discussions of the effects of other size distributions can be found, for instance, in Cotton and Anthes (1989). The quantities  $\rho_r$  ( $\approx 10^3 \text{ kg m}^{-3}$ ) and  $\rho_i$  are the densities of water and ice, respectively. The density of ice particles depends on the moisture available during the growth process and on the size of the collected drops. Furthermore, the density of the ice depends on the time required for freezing of the collected cloud droplets or rain drops. Therefore, a wide range of this density is documented in the literature. Zikmunda and Vali (1972), for instance, report values of 250–700  $\text{kg m}^{-3}$  for conical graupel, Locatelli and Hobbs (1974) values of 20–270  $\text{kg m}^{-3}$  for densely rimed columns and 50–450  $\text{kg m}^{-3}$  for lump graupel (see also Pruppacher and Klett, 1980). As in our study the collection of ice by rain drops is not considered, which would lead to higher densities of ice, and as the mean diameters of the ice nuclei which are considered in the parameterizations of the riming and sedimentation processes range between 0.8 and 3.2 mm (Locatelli and Hobbs, 1974), a value of 84  $\text{kg m}^{-3}$  was chosen, in accord with Heymsfield and Sabin (1989). As reported by these authors, the density of ice decreases from 700 to 84  $\text{kg m}^{-3}$  as the diameter of the ice crystals increases from 0.1 to 0.2 mm. Above 0.2 mm the density of ice retains the value of 84  $\text{kg m}^{-3}$ . The influence due to higher values of  $\rho_i$  will be discussed later.

Note that the use of a massweighted mean terminal velocity results in an overprediction of the sedimentation at the beginning of precipitation formation as all sizes, even the very large ones which have not been formed at that time, are taken into account.

Many authors do not use the density weighted correction term because of its inaccuracy. Beard (1977) showed that this correction is only useful for large drops ( $D > 3 \text{ mm}$ ); more complicated correction formulas are of value for smaller drops. The influence of this correction term and the choice of  $N_{oi}$  will be discussed later.

To avoid that the fallout term (last term of Eq. 1) becomes computationally instable in the shallow layers of the atmospheric boundary layer (ABL) when a larger time step is used, this term is determined after all other processes are predicted. This procedure ensures that only the rainwater and ice present at that time in a model layer can fall out of this layer.

### 2.1. Condensation and deposition

Essential aspects of clouds are the release of latent heat and the consumption of heat which are connected with phase transition processes as well as the interrelation between microphysics and dynamics. Obviously, the condensation and/or water vapor deposition rates have to be determined. Frequently, a diagnostic procedure like the well-known saturation adjustment is utilized in cloud models to avoid a considerable time consumption which is required when these transition processes are predicted. In our study the following saturation adjustment is used to determine the mixing ratios for water vapor, cloud water, and ice (Lord et al., 1984):

$$q_s = \begin{cases} q_{sw}, & \text{if } q_c \geq 0 \text{ and } q_i = 0 \\ q_{si}, & \text{if } q_i > 0 \text{ and } q_c = 0, \\ \frac{q_c q_{sw} + q_i q_{si}}{q_c + q_i}, & \text{if } q_c > 0 \text{ and } q_i > 0 \end{cases} \quad (6)$$

where in the case, when both cloud water and ice are present, the saturation mixing ratio,  $q_s$ , is assumed as a massweighted mean of the saturation mixing ratio with respect to water,  $q_{sw}$ , and ice,  $q_{si}$ , respectively.

In saturated air masses at temperatures lower than  $T_{oo} = -35^\circ\text{C}$  only ice and at temperatures warmer than  $T_o = 0^\circ\text{C}$  only cloud water is formed. In the temperature range between  $T_{oo}$  and  $T_o$  ice and supercooled water may coexist so that under supersaturated conditions water vapor deposition and condensation is partitioned between cloud water and ice as a linear function of temperature. Thus, the condensation/deposition rate is given by

$$CD_{vk} = \begin{cases} (q_v - q_{sw}) r_{vc} / \delta t & \text{for } T > 0^\circ\text{C} \\ (q_v - q_s) \Delta T_k r_{vk} / \delta t & \text{for } 0^\circ\text{C} \leq T \leq T_{oo}, \\ (q_v - q_{si}) r_{vi} / \delta t & \text{for } T < T_{oo} \end{cases} \quad (7)$$

where  $k$  stands for  $c$  and  $i$ , respectively. The parameter  $\delta t$  is the time step (usually 120 s in our studies),  $\Delta T_c = (T - T_{oo}) / (T_o - T_{oo})$ ,  $\Delta T_i = (T_o - T) / (T_o - T_{oo})$ ,  $r_{vc}$  and  $r_{vi}$  stand for  $[1 + L_c^2 q_s / (R_v c_p T^2)]^{-1}$  and  $[1 + L_s^2 q_s / (R_v c_p T^2)]^{-1}$ , respectively, and  $R_v$  is the gas constant for water vapor. Note that the results of a study using  $-40^\circ\text{C}$  as the lower limit for coexistence show only slight differences in the rainwater, cloud water and precipitation fields in comparison with that using  $-35^\circ\text{C}$ . The reason for this is that at low temperatures ice is preferably formed (see also Fig. 1).

If the air is subsaturated with respect to water and supersaturated with respect to ice, the so-called Bergeron–Findeisen-process is effective, i.e., cloud water evaporates and the released water vapor deposits on ice crystals. Therefore, under subsaturated conditions the cloud water evaporates before ice sublimates.

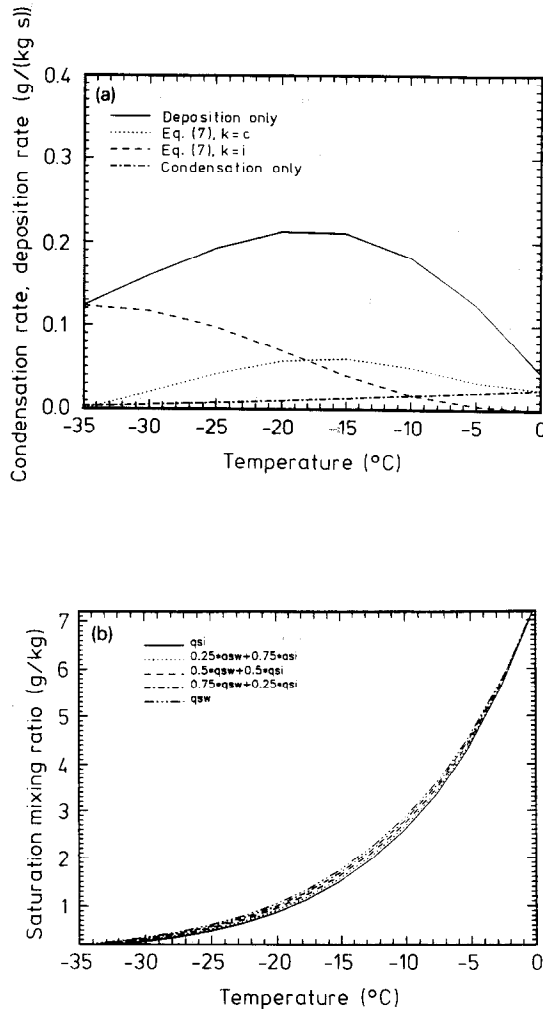


Fig. 1. (a) Condensation and deposition rates and (b) the saturation mixing ratios of ice and water as well as the massweighted mixing ratio in dependence on temperature. For (a) the mixing ratios of the already present cloud water and ice depend linearly on temperature and the air is supersaturated with respect to water by 1%.

Fig. 1a shows that at low supercooling the partitioning of supersaturation according to Eq. (7) leads to a slight water vapor deposition and much higher condensation rates. These condensation rates are slightly higher than those of condensation alone and the deposition rates are much lower than those of deposition alone. The assumptions on the saturation mixing ratio and on the partitioning between cloud water and ice lead to a slight subsaturation of mixed phase clouds with respect to water and supersaturation with respect to ice (Fig. 1b). It can be derived from Fig. 1 that ice-phase related latent heating gains importance at those levels of the atmosphere where the condensation and, hence, the condensational

heating is greatly reduced. Obviously, at low temperatures the ice formation prevails. Hence, the massweighted saturation mixing ratio shifts towards the ice saturation mixing ratio. Note that  $q_s \approx q_{si}$  for  $q_i \gg q_c$  and  $q_s \approx q_{sw}$  for  $q_c \gg q_i$  for all temperatures.

### 2.2. Autoconversion and accretion

Once cloud water is present, rainwater can be formed by autoconversion and accretion. The autoconversion rate can be written as (e.g., Kessler, 1969; Anthes et al., 1987):

$$CN_{cr} = \begin{cases} \alpha(q_c - q_{co}) & \text{if } q_c \geq q_{co} \\ 0 & \text{if } q_c < q_{co} \end{cases} \quad (8)$$

The onset of autoconversion is controlled by the parameters  $\alpha = 10^{-3} \text{ s}^{-1}$  and  $q_{co} = 0.5 \text{ g/kg}$  which are used here, in accord with Anthes et al. (1987). As pointed out by these authors,  $\alpha$  and  $q_{co}$  are grid-dependent. The choice of  $\alpha$  is only of importance during the onset of rainwater formation which depends on  $q_{co}$ . Note that the higher the value of  $q_{co}$  is chosen, the later precipitation is formed or even may be suppressed.

Accretion only occurs, when rainwater has already been formed. Assuming a Marshall–Palmer distribution for the raindrops and continuous collection, the accretion rate can be expressed by (Orville and Kopp, 1977; Anthes et al., 1987):

$$CL_{cr} = E_r \frac{\pi N_{or} a_r \Gamma(3 + b_r) q_c}{4\lambda_r^{3+b_r}}, \quad (9)$$

where  $E_r$  is the collection efficiency which is usually set equal to 1 because for encounters between large fast-falling rain drops and very small (cloud) drops, the collection efficiency approaches unity. The assumption of continuous collection is an idealization as collection depends on the radius of the drops and on hydrodynamic forces. Note that more accurate  $E_r$ -values can be estimated using the potential flow solution (e.g., Tripoli and Cotton, 1980). But this procedure requires much more CPU-time. Lower values of  $E_r$  may lead to higher amounts of cloud water and, hence, higher autoconversion rates. Moreover, larger riming rates may also be achieved.

### 2.3. Evaporation of rainwater

Rainwater falling through the cloud base begins to evaporate. The evaporation of rain drops can be written by (Orville and Kopp, 1977; Anthes et al., 1987)

$$EV_{rv} = \frac{2\pi(1 - q_v/q_{sw})N_{or}\{0.78\lambda_r^{-2} + 0.32S_c^{1/3}\Gamma[(b_r + 5)/2]a_r^{1/2}\nu^{-1/2}\lambda_r^{-(b_r + 5)/2}\}}{\rho_a[L_v^2/(K_a R_v T^2) + 1/(\rho_a q_{sw} D_v)]}, \quad (10)$$

where  $\nu$  is the kinematic viscosity of the air,  $K_a$  is the thermal conductivity,  $D_v$  is the diffusivity for water vapor, and  $S_c = \nu/D_v$  is the Schmidt number.

### 2.4. Riming

Several authors (e.g., Koenig and Murray, 1976; Cotton et al., 1982) assume that the ice crystal growth processes could be described by the growth of a mean ice crystal. Cotton et

al. (1982) distinguish between the ice crystal growth by riming on hexagonal plates, on slightly rimed hexagonal plates, and on graupel-like hexagonal particles. The ice crystal type is defined by its mass  $m_i$ ,

$$m_i = \rho_a q_i / N_i, \quad (11)$$

where  $q_i$  is predicted, and  $N_i$  is the ice nuclei concentration which is determined by the Fletcher (1962) formula

$$N_i = A \exp(\beta(T_o - T)), \quad (12)$$

with  $T < T_o$ . Values of  $\beta$  range from 0.4 to 0.8  $\text{K}^{-1}$ . Usually the value of  $\beta$  is 0.6  $\text{K}^{-1}$  as used in our studies. The quantity  $A$  is more variable, typically being  $10^{-2} \text{ m}^{-3}$ , with variations of several orders of magnitude sometimes occurring (Fletcher, 1962). If  $D_i$  and  $u_i$  represent the diameter and the fall velocity of the mean ice crystal, these quantities are related to the mean mass by

$$D_i = k_1 m_i^{1/2} \quad (13)$$

$$u_i = k_2 D_i (\rho_o / \rho_a)^{1/2}, \quad (14)$$

where  $k_1$  and  $k_2$  are given by (Hobbs et al., 1972)

$$\left. \begin{array}{l} k_1 = 16.3 \text{ m kg}^{-1/2} \\ k_2 = 304 \text{ s}^{-1} \end{array} \right\} \text{if } m_i < 1.7 \cdot 10^{-10} \text{ kg}$$

for hexagonal plates and

$$\left. \begin{array}{l} k_1 = 6.07 \text{ m kg}^{-1/2} \\ k_2 = 1250 \text{ s}^{-1} \end{array} \right\} \text{if } 1.7 \cdot 10^{-10} \text{ kg} \leq m_i < 10^{-8} \text{ kg.}$$

for slightly rimed hexagonal plates. For graupel-like snow of hexagonal type with masses  $> 10^{-8} \text{ kg}$  and diameters less than 2.8 mm, the diameter and fall velocity are referred to the mean mass by (Locatelli and Hobbs, 1974)

$$D_i = k_1 m_i^{0.417} \quad (15)$$

$$u_i = k_2 D_i^{1/4} (\rho_o / \rho_a)^{1/2}, \quad (16)$$

where  $k_1 = 1.58 \text{ m kg}^{-0.417}$  and  $k_2 = 4.84 \text{ m}^{3/4} \text{ s}^{-1}$ . The riming rate due to the collection of cloud drops by ice crystals is calculated by (Cotton et al., 1982)

$$CL_{ci} = E_i u_i N_i q_c \pi D_i^2 / 4, \quad (17)$$

where  $E_i$  is the collection efficiency. Since the characteristic efficiency for plates riming small cloud droplets cannot be obtained in a straight forward manner, Cotton et al. (1982) assume a sphere of diameter equivalent to a hexagonal plate and stokes flow about the plate for calculating the collection efficiency. Other authors assume continuous collection (e.g., Lin et al., 1983). For simplification, in our study  $E_i$  was chosen as equal to 0.8. Lower values of  $E_i$  may lead to lower riming rates and, hence, less cloud water consumption by riming. Thus, more cloud water is available for autoconversion or accretion. The opposite is true for higher values of  $E_i$ . Note that riming, accretion and autoconversion are competitive processes.

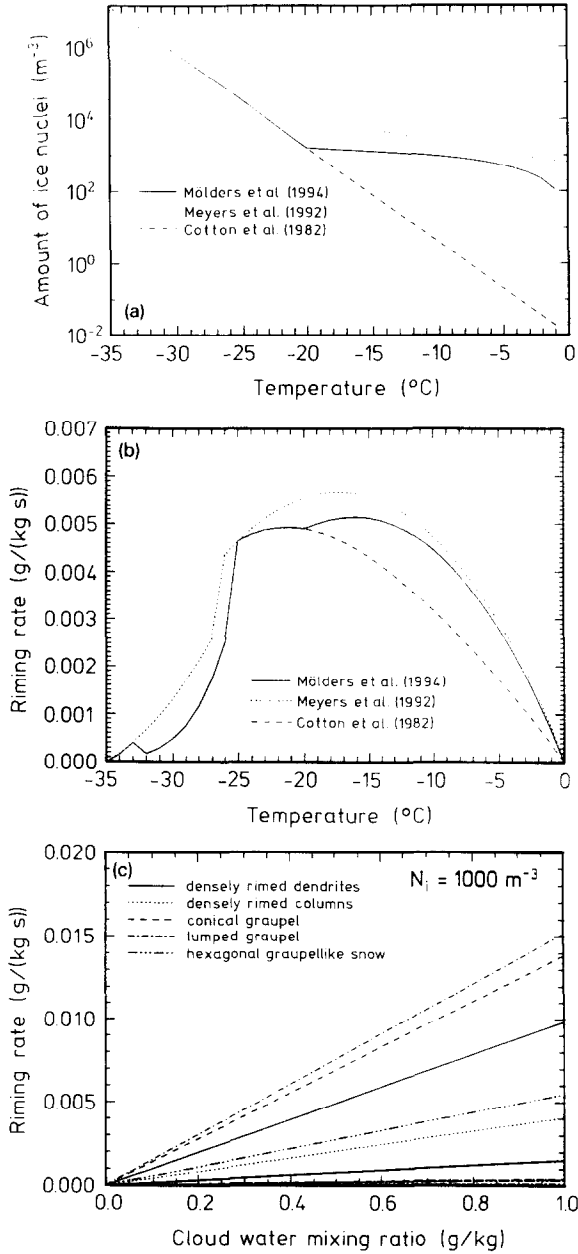


Fig. 2. Dependence of (a) ice nuclei concentration and (b) related riming rate on temperature. The ice nuclei concentrations are determined assuming a temperature gradient of 6.7 K/km with the freezing level in 2.2 km and that the water vapor mixing ratio equals the saturation mixing ratio of water. The mixing ratios of the cloud water and ice already present depend linearly on temperature. Peaks in the riming rates occur when passing from one ice crystal class to another. (c) Riming rates for the maximum (upper curve) and minimum (lower curve) diameter of different types of ice crystals.

The Fletcher formula (Eq. 12) tends to overpredict ice crystal concentrations in very cold clouds and to underpredict the ice crystal concentration at temperatures warmer than  $-10^{\circ}\text{C}$  as much as three or four orders of magnitude (e.g., Pruppacher and Klett, 1980; Cotton and Anthes, 1989). To consider the sensitivity to saturation conditions and to avoid the overprediction at low temperatures, Cotton et al. (1986) combined the Fletcher formula with the Huffman (1973) equation for the relative supersaturation dependence of ice nucleation to determine the ice nuclei concentration. A similar formulation was used by Meyers et al. (1992). Since at temperatures near the lower limit of the coexistence range usually only few cloud water is formed, it seems to be sufficient to correct the Fletcher formula for the range in the vicinity of the freezing point. In our study a minimum amount of  $N_i = \rho_a q_i / 2.49 \times 10^{-7} \text{ m}^{-3}$  is assumed to avoid too low ice nuclei concentrations at small degrees of supercooling which can cause ice crystals becoming too large (of up to several decimeters) and, hence, decrease the riming rate. This minimum value of  $N_i$  is based on the restriction of the range, for which Eqs. (15) and (16) are only valid, by the uppermost diameter of 2.8 mm. As shown in Fig. 2, this formulation results in an increase of ice nuclei concentration at low supercooling and, hence, in higher riming rates than the original Fletcher formula used by Cotton et al. (1982). The use of the “restricted” Fletcher formula slightly improves the forecasts. Simulations using the original Fletcher formula provide higher cloud water mixing ratios and lower ice mixing ratios than those predicted by simulations using the restriction. Due to the release of latent heat during freezing and the consumption of heat during melting and evaporation differences especially in the calculated temperature fields occur in the riming and melting regions.

The riming procedure can be extended to other ice crystal forms such as dendrites, conical or lumped graupel. Fig. 2b illustrates that the riming rate significantly changes when passing from one ice crystal class to another. If we assume that all these forms of ice crystals exist and that the ice nuclei concentration,  $N_i$ , is equal to  $1000 \text{ m}^{-3}$ , the riming procedure may lead to higher or lower riming rates than that for hexagonal graupel-like snow which has the highest riming rate in our parameterization scheme (Fig. 2). Densely rimed columns, for example, would lead to lower riming rates. Since in the temperatures range between  $-10^{\circ}\text{C}$  and  $-20^{\circ}\text{C}$  at saturation conditions near water saturation ice crystals of hexagonal type are the most frequent (e.g., Laube and Höller, 1988) it seems to be sufficient to take hexagonal plates, slightly rimed hexagonal plates, and graupel-like hexagonal particles into account. It is possible that the riming process may be underestimated by parameterization schemes as used in this study.

### 2.5. Melting

Ice crystals falling through the freezing level melt. In contrast to Dudhia (1989) and Cotton et al. (1982) who assumed that all ice crystals completely melt when falling through the level of freezing, in our study ice can exist for some time in warmer layers until it melts finally. It is assumed that the melted mass is converted into rain drops. The melting rate is formulated similar to Cotton et al. (1982) by

$$ML_{ir} = q_i / \delta t. \quad (18)$$

More sophisticated parameterizations of the melting process, where hydrodynamical and shedding effects, saturation and evaporative cooling are taken into consideration, as often done in cloud models of mesoscale  $\beta$  and  $\gamma$ , would increase rapidly the computational efforts. Evaporative cooling, for instance, slows the melting. Since only one ice class is considered in our parameterization, ice-aggregate and/or aggregate–aggregate collection are not included. Note that aggregates survive greater fall distances before melting is completed (Willis and Heymsfield, 1989).

### 3. Results

The model domain encompasses the troposphere up to the 100 hPa level over Europe with a horizontal grid resolution of 80 km  $\times$  80 km (46  $\times$  61 grid points) and 15 non-equidistant  $\sigma$ -levels (8 levels below and 7 levels above 2 km) in the vertical direction. The initial data to start the simulations were derived from objective analysis of the NMC data. Since cloud water, rainwater and ice are not included in the analysis and in the assimilation scheme, the simulations start without initial values of these parameters. (The values of these parameters, of course, are also set to zero at the boundaries.) In view of this fact, some spin-up time is required to form water substances as well as precipitation.

A three day episode from 25th April 1200 GMT to 28th April 1986 1200 GMT was chosen to study the effects of parameterized microphysics on the cloud structures, dynamics and precipitation. The meteorological situation during that time was governed by a cyclone near Iceland and high pressure over northeastern Europe. Over the Alps a low pressure system caused heavy rainfalls. On April 25th the weather situation in Europe showed little pressure gradients. In front of a trough laying over western Europe warm air masses were advected from southwest. The low located over Iceland decreased and moved slowly eastwards; the low located over the Alps enforced and moved northwards accompanied by heavy rainfall over southern Germany during the 26th April. On the 27th April the low moved from northern Germany towards the North Sea. A new cyclone came from the Adriatic Sea moving northwards. Again strong precipitation was registered in southern Germany. Satellite data show high amounts of ice clouds during this episode.

Results of simulations using the ice parameterization described above with and without riming being activated, denoted as COLD and NOR, respectively, are presented and discussed. Since the ice parameterization scheme is an extension and modification of the warm scheme the results of the COLD run are compared with those of a simulation considering the warm processes only (WARM) to examine the influence of the ice processes. Several experiments have been performed in order to investigate the sensitivity of the model to different parameters and processes. Furthermore, a Berry-type autoconversion was tested. Three-dimensional fields of wind, temperature and the mixing ratios of water vapor, cloud water, rainwater and ice (if included) as well as the surface temperatures, surface pressure, rain and snow rate are predicted.

At first, general remarks on the results of the simulations are given before the results of the COLD simulation are evaluated and discussed. Later the results of the sensitivity studies are presented and compared with those of the COLD run if not indicated otherwise.

Table 1

Persistence (Persist), initial error and the RMS errors of the WARM, COLD and NOR runs after 72 h of simulation

| pressure level                                    | WARM | COLD | NOR  | Persist | Initial Error |
|---|------|------|------|---------|---------------|
| <b>RMS wind errors (m/s)</b>                      |      |      |      |         |               |
| 1000 hPa  | 5.3  | 5.3  | 5.2  | 9.4     | 1.0           |
| 850 hPa   | 5.7  | 5.7  | 5.7  | 11.8    | 0.5           |
| 700 hPa   | 6.1  | 6.2  | 6.1  | 15.0    | 0.5           |
| 500 hPa   | 11.0 | 11.1 | 11.1 | 24.5    | 1.0           |
| 300 hPa   | 16.1 | 16.5 | 16.4 | 43.5    | 2.5           |
| <b>RMS temperature errors (K)</b>                 |      |      |      |         |               |
| 1000 hPa  | 2.4  | 2.6  | 2.6  | 3.5     | 0.2           |
| 850 hPa   | 1.9  | 1.9  | 2.0  | 4.7     | 0.1           |
| 700 hPa   | 1.7  | 1.6  | 1.7  | 5.9     | 0.1           |
| 500 hPa   | 3.2  | 3.2  | 3.2  | 7.7     | 0.2           |
| 300 hPa   | 3.8  | 3.8  | 3.8  | 7.2     | 0.3           |
| <b>RMS height errors (m)</b>                      |      |      |      |         |               |
| 1000 hPa  | 19.5 | 19.5 | 19.8 | 77.5    | 0.7           |
| 850 hPa   | 17.9 | 18.3 | 18.3 | 78.1    | 0.8           |
| 700 hPa   | 22.2 | 23.1 | 23.1 | 96.6    | 1.5           |
| 500 hPa   | 39.4 | 39.3 | 39.8 | 154.7   | 3.8           |
| 300 hPa   | 51.6 | 52.9 | 52.7 | 208.1   | 2.5           |
| <b>RMS water vapor mixing ratio errors (g/kg)</b> |      |      |      |         |               |
| 1000 hPa  | 1.6  | 1.7  | 1.6  | 2.1     | 0.4           |
| 850 hPa   | 1.4  | 1.5  | 1.4  | 1.6     | 0.1           |
| 700 hPa   | 1.0  | 1.0  | 1.0  | 1.2     | 0.1           |
| 500 hPa   | 0.4  | 0.4  | 0.4  | 0.4     | 0.0           |
| 300 hPa   | 0.1  | 0.0  | 0.0  | 0.0     | 0.0           |

Synoptic-scale models have been verified over the years by calculation of objective indices or scores that reflect the skill in forecasting the mass, pressure or geopotential height fields and the precipitation occurrence and amount (Anthes, 1983). The calculated measures of skill for temperature, wind vector, geopotential height, sea level pressure only hardly differ for the simulations and, hence, do not allow to indicate which simulation is the best. In view of the low differences in the measures of skill only those of the WARM, COLD and NOR simulations which are the simulations with the largest differences to each other are listed in Tables 1 and 2. Since the range of the  $S_1$ -scores for the sea level pressure between essentially perfect and worthless forecasts is 30 to 80 (Anthes, 1983), all forecasts can be considered as acceptable for this quantity. Typical RMS wind vector errors are 3 to 8 m s<sup>-1</sup>, geopotential height errors of 20 to 50 m, and temperature errors of 1.5 to 4.5 K for a 72 h forecast (Anthes et al., 1989). With respect to these measures of skill all simulations provide acceptable results. It seems that in the regions between the surface and the 500 hPa-level the model performs better than in the upper troposphere. The low vertical resolution or errors in the observations may be a reason. Note that in Europe different types of radiosondes are used which may artificially cause gradients in the observed fields (Phillips et al., 1981). The verifying analyses of the water vapor mixing ratio are even less accurate than those of other variables, because of smaller-scale features present in the humidity fields (Anthes et al., 1989). The measures of skill concerning the results of the water vapor and the precipitation distribution show more variance between the different simulations than

Table 2

 $S_1$ -scores for the geopotential height for the WARM, COLD and NOR runs after 72 h of simulation

| pressure level | WARM | COLD | NOR  | Persist | Initial Error |
|----------------|------|------|------|---------|---------------|
| 1013 hPa       | 25.6 | 25.0 | 25.6 | 41.8    | 12.3          |
| 1000 hPa       | 45.1 | 44.1 | 45.1 | 88.5    | 3.7           |
| 850 hPa        | 38.6 | 38.3 | 38.8 | 93.4    | 3.8           |
| 700 hPa        | 36.4 | 36.7 | 37.1 | 93.6    | 4.8           |
| 500 hPa        | 36.7 | 36.8 | 36.9 | 98.9    | 6.9           |
| 300 hPa        | 38.9 | 40.1 | 40.3 | 109.0   | 3.1           |

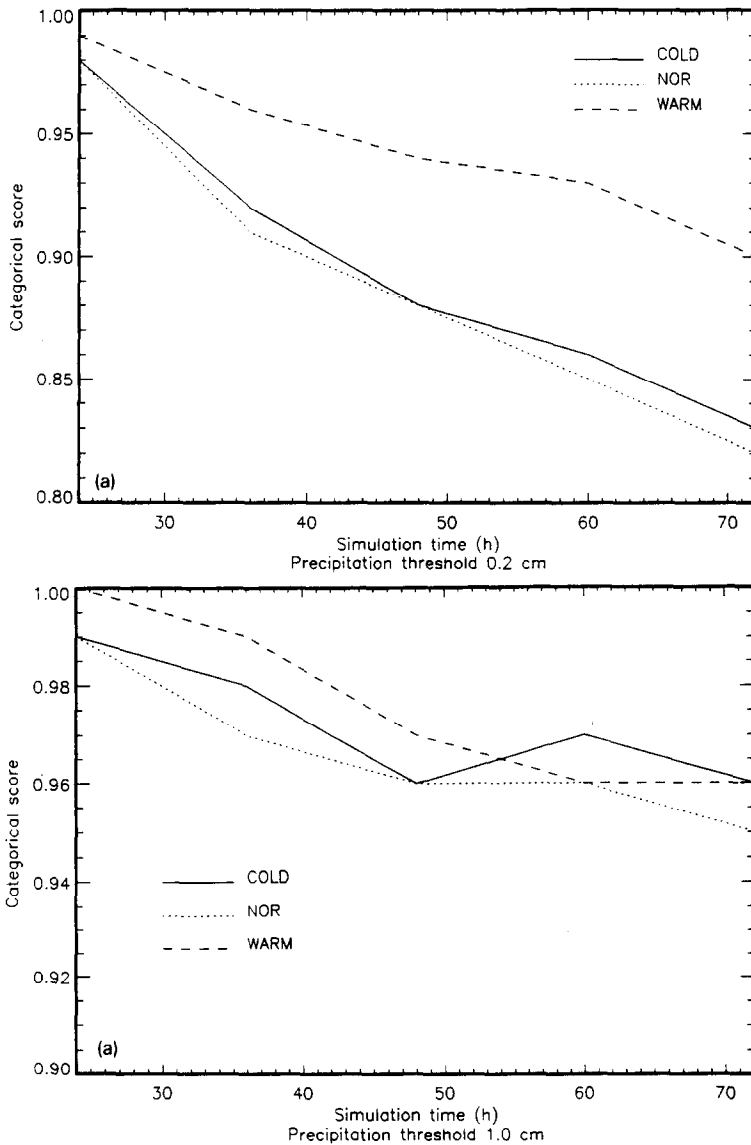
those discussed above. Again they differ the largest for the WARM, COLD and NOR simulations (Tables 1, 2, Fig. 3).

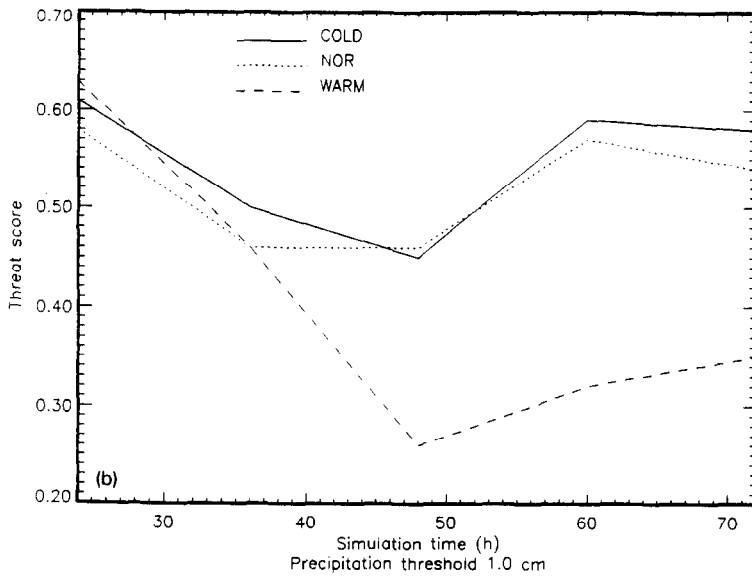
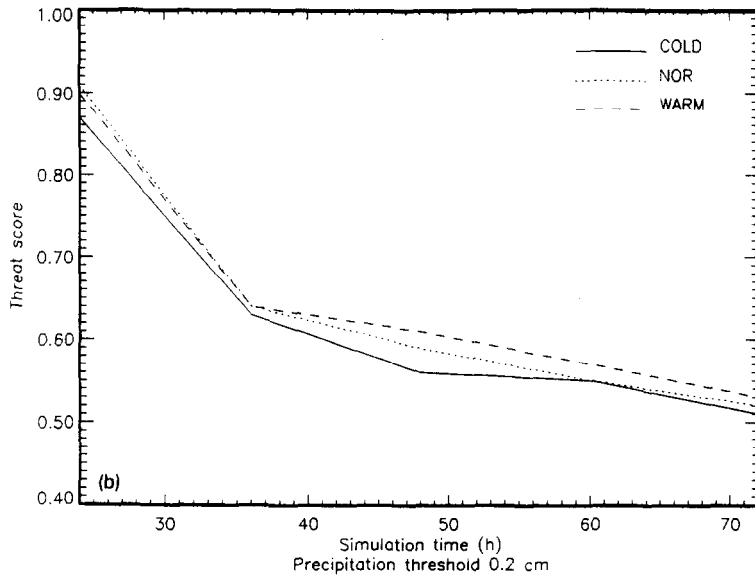
After 72 h of simulation time all forecasts show differences in the location of the cloud systems. In comparison with NOAA9 satellite data, all simulations produce a temporal offset of about two hours in the location of the predicted cloud systems, i.e., the positions of the cloud fields predicted for the time two hours after the satellite passage match at best with the positions observed from the satellite during its passage. The reasons for this temporal offset may result from the neglect of further subscale and microphysical processes. (see also Mölders et al., 1994). This offset may also be responsible for most of the differences between the analysis and the weather predictions. Note that the cloud distribution predicted by the WARM simulation has to be considered as poor at the end of the simulation as large amounts of clouds were predicted in the area over the anticyclone over Russia, where only some fair weather clouds were observed.

Compared with the analysis, the wind fields show their largest differences in the regions of the cloud systems for all simulations. As an example for the weather situation on 28th April 1986, 1200 GMT the analysis of the geopotential height, the temperature and the wind fields are shown for the 750 hPa level in Fig. 4. (Since the Alps exceed the 850 hPa level, the 750 hPa level was used for the purposes of comparison.) This figure also shows the corresponding fields predicted by the COLD simulation. Note that the results of the other runs are similar. The maximum differences in wind speed amount to  $5 \text{ m s}^{-1}$  (and more), especially large differences between the predicted wind fields and the analysis are found over southern France and eastern Germany. Winds from southeast, for example, are predicted for eastern Germany while winds from southwest are given by the analysis. In the region of the North Sea the wind speeds are underpredicted (Fig. 4).

Obviously, discrepancies between the observed fields of wind and geopotential height are mirrored in the vertical motions. The predicted wind circulation differs significantly from that of the analysis (Figs. 5, 6, 7 and 9). The wind circulation fields predicted by the simulations using the ice parameterization scheme agree better with that of the analysis than the wind circulation fields provided by the WARM simulation (Fig. 7), but also these predictions are not satisfying. Figs. 5, 6, 7 and 9 also illustrate that at some locations in the cloudy regions the vertical velocities are directed downward for the simulations while there are upwards motions in the analysis and vice versa. The largest differences occur over complex terrain (e.g., over the Alps). Little differences in the vertical velocity are found under anticyclonic conditions.

Fig. 4 also shows that differences between the predicted and analyzed temperature fields occur. The temperature minima at the 750 hPa-level, for instance, are predicted northwards of their position analyzed. The temperatures in 500 hPa are underpredicted. However, although the temperature values of the minima and maxima of the prediction and the analysis differ from each other in this level, they are predicted at the right places. The predicted horizontal temperature gradients are often stronger than those of the analysis.





Besides the wind circulation fields, Fig. 5 shows the analysis of the relative humidity. Areas of high relative humidity are found over the Alps and Scandinavia reaching up to the 300 hPa level. Generally, for all simulations the predicted relative humidity is too high in comparison with the analysis.

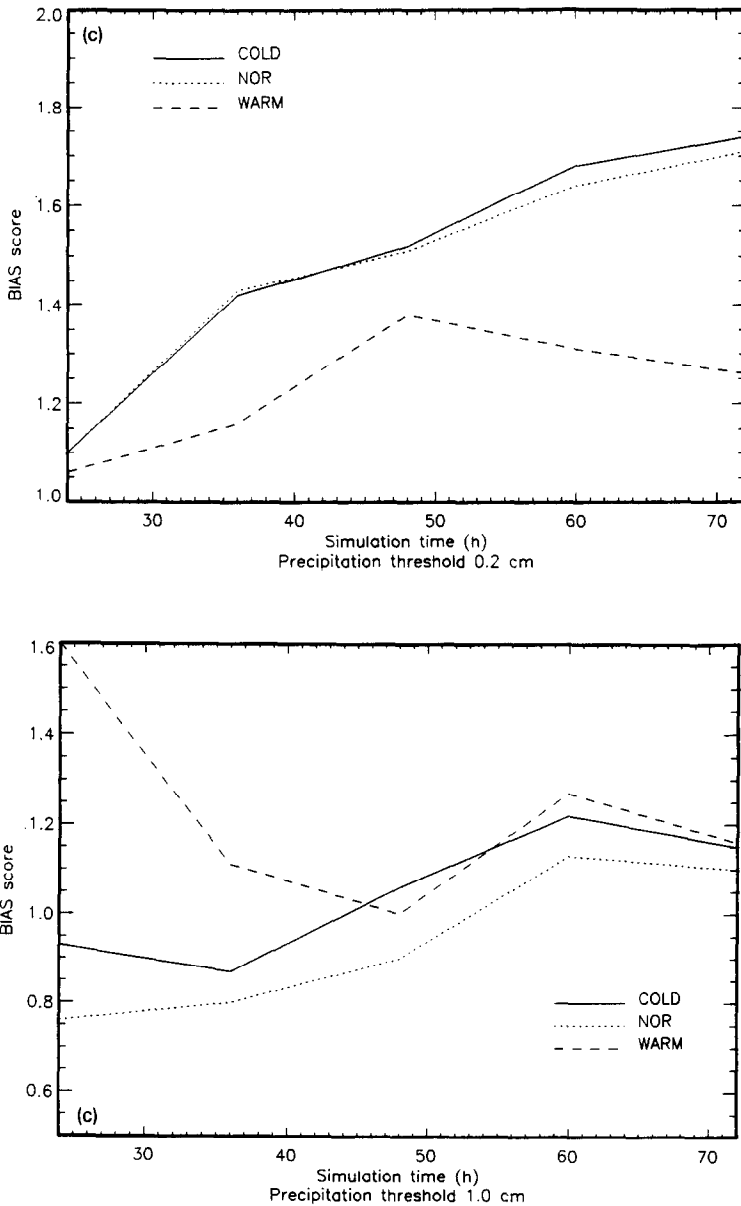


Fig. 3. Temporal development of (a) categorical score, (b) threat score and (c) BIAS score determined for the WARM, COLD and NOR simulations considering threshold amounts of 0.2 cm and 1.0 cm. Note that no precipitation data were available before 26th April 1986, 600 GMT.

3.1. Simulation with ice processes (COLD)

The relative humidity and the wind circulation predicted by the COLD simulation are presented in Fig. 6. As already mentioned, a significant offset in the position of the humid areas both predicted and analyzed can be found.

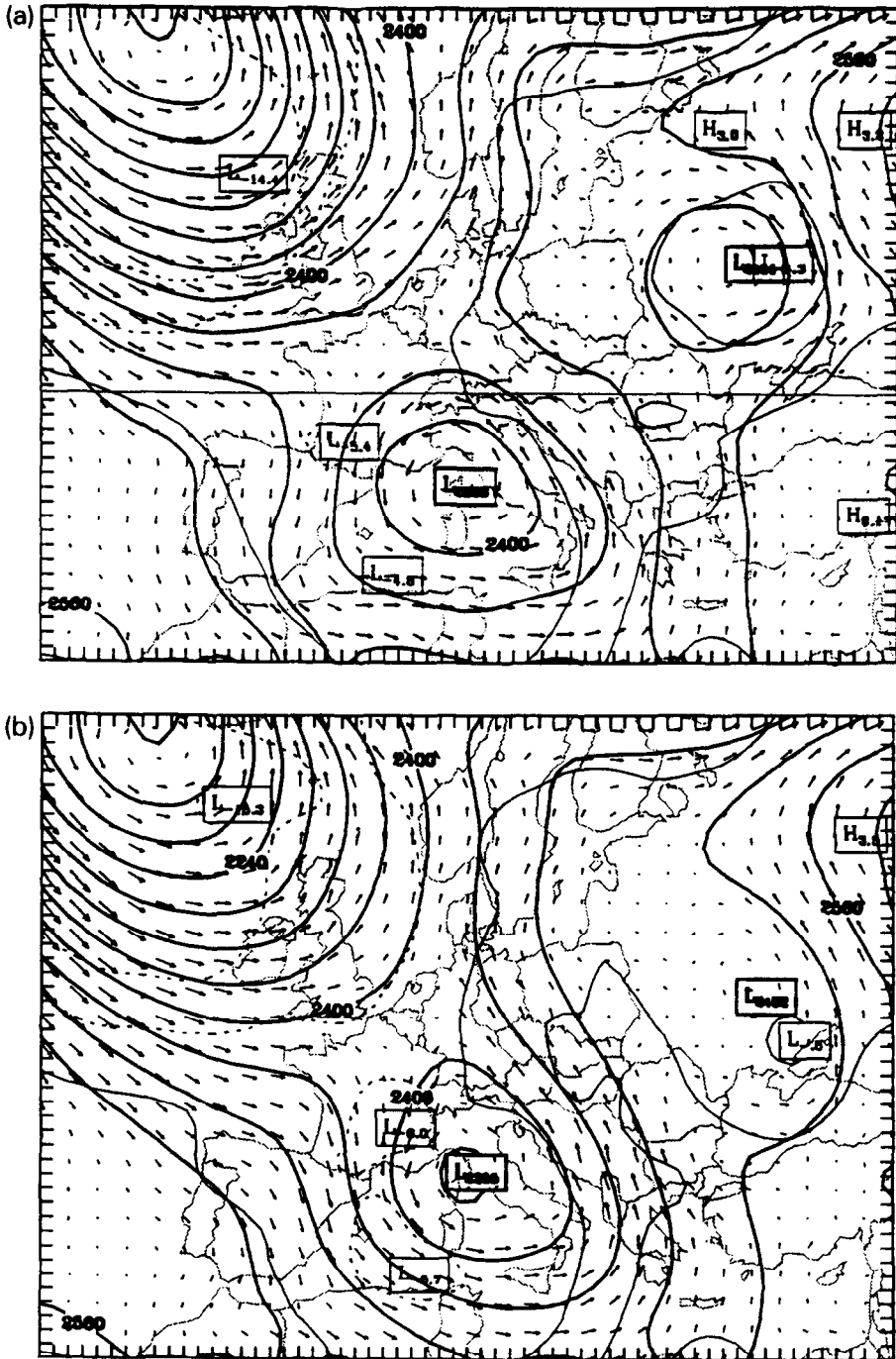


Fig. 4. Fields of geopotential height in 750 hPa (thick lines), temperature (thin and dashed lines) and wind (vector arrows) for 28th April 1986, 1200 GMT. (a) Analysis and (b) as predicted by the COLD simulation. Contour lines range from  $-10$  to  $10^{\circ}\text{C}$  by steps of  $5^{\circ}\text{C}$ , and from 2100 to 2600 m by steps of 40 m. The maximum wind speed is  $28.1\text{ m s}^{-1}$ . The thick line indicates the cross section presented in Figs. 5, 6, 7 and 9.

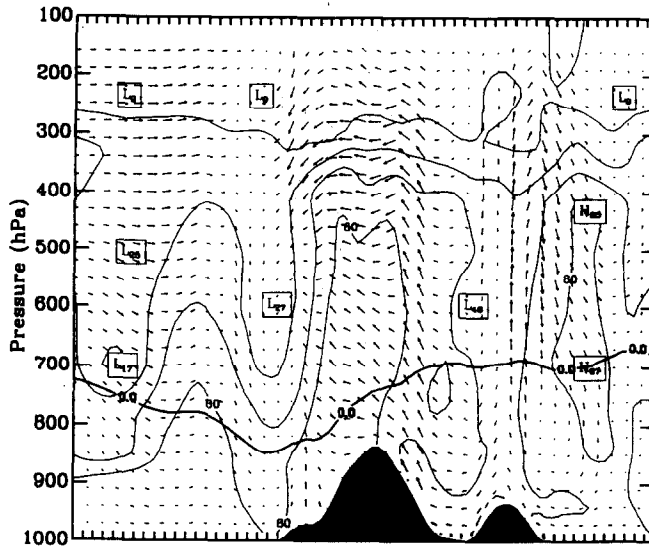


Fig. 5. West-east cross section (as indicated in Fig. 4) from the Gulf of Biscay over the Alps to the Black Sea and from the surface to the model top (100 hPa). Analysis for 28th April 1986, 1200 GMT. Relative humidity is displayed by the isolines. The fat solid line gives the 0°C-isotherm. Arrows represent the wind circulation projected into the cross section. Maximum wind speeds in the horizontal and vertical direction are  $27.55 \text{ m s}^{-1}$  and  $0.063 \text{ Pa s}^{-1}$ .

The COLD simulation provides ice clouds, water clouds and mixed phase clouds (Fig. 6). Some clouds are completely glaciated in their upper parts. Here, the ice mass is very low with terminal velocities less than  $2 \text{ m s}^{-1}$ . In some grid columns clouds occur in different atmospheric layers. Fig. 6 illustrates that clouds also exist in undersaturated areas until they completely evaporate. Ice falling in levels warmer than 0°C melts and forms rainwater (Fig. 6). Note that only precipitation data were available for comparison. However, the predicted ice content and liquid water content of the clouds, are within the frame of what is usually observed.

The rain forecast of the COLD simulation agrees broadly with the precipitation data of Scheele and Verver (1990) in temporal sequence, pattern and rain rates. The 72 h accumulated precipitation rates are overestimated (Mölders et al., 1994), especially over the Alps. The differences are ascribable to the poor resolution of the model as well as to subscale phenomena caused by the orography (e.g., mountain-valley-circulation-systems) which may modify the wind circulation, and, hence, influence the formation of rain. Such orographically induced subgrid effects cannot be taken into account because of the poor horizontal resolution of the mesoscale  $\alpha$  weather forecast models. Moreover, in the model a grid averaged altitude of the terrain within a grid box is used to represent the terrain height.

### 3.2. Simulation without ice processes (WARM)

The WARM simulation leads to less structured vertical motions than the COLD run (Figs. 6 and 7). The comparison of the results obtained from these simulations shows that

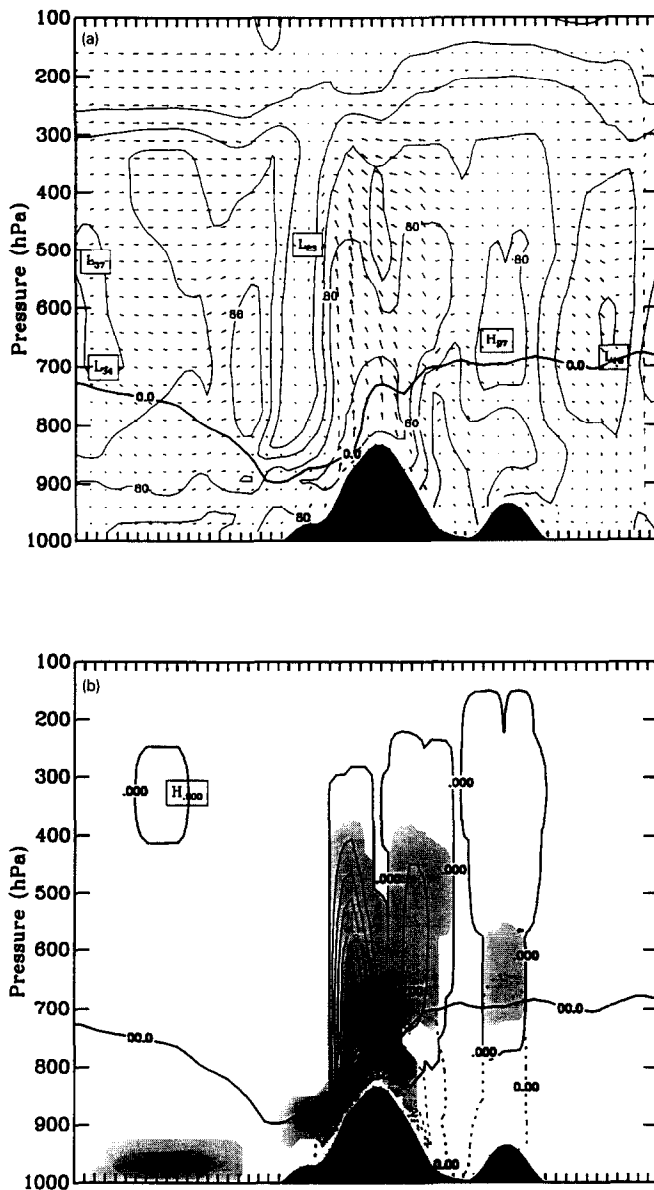


Fig. 6. (a) As Fig. 5, but for the COLD simulation. Maximum wind speeds in the horizontal and vertical direction are  $26.40 \text{ m s}^{-1}$  and  $0.110 \text{ Pa s}^{-1}$  (from Mölders and Laube, 1994). (b) Predicted mixing ratios for cloud water (shaded areas), rainwater (dashed lines), and ice (solid lines) (with reference to Mölders and Laube, 1994). Contour lines range from 0.001 to 2.2 g/kg by steps of 0.05 g/kg for rainwater and from 0.001 to 0.75 g/kg by steps of 0.05 g/kg for ice, respectively. Grey levels are at 0.001, 0.05, 0.1, 0.15, 0.2, 0.25, 0.35 and 0.4 g/kg, respectively.

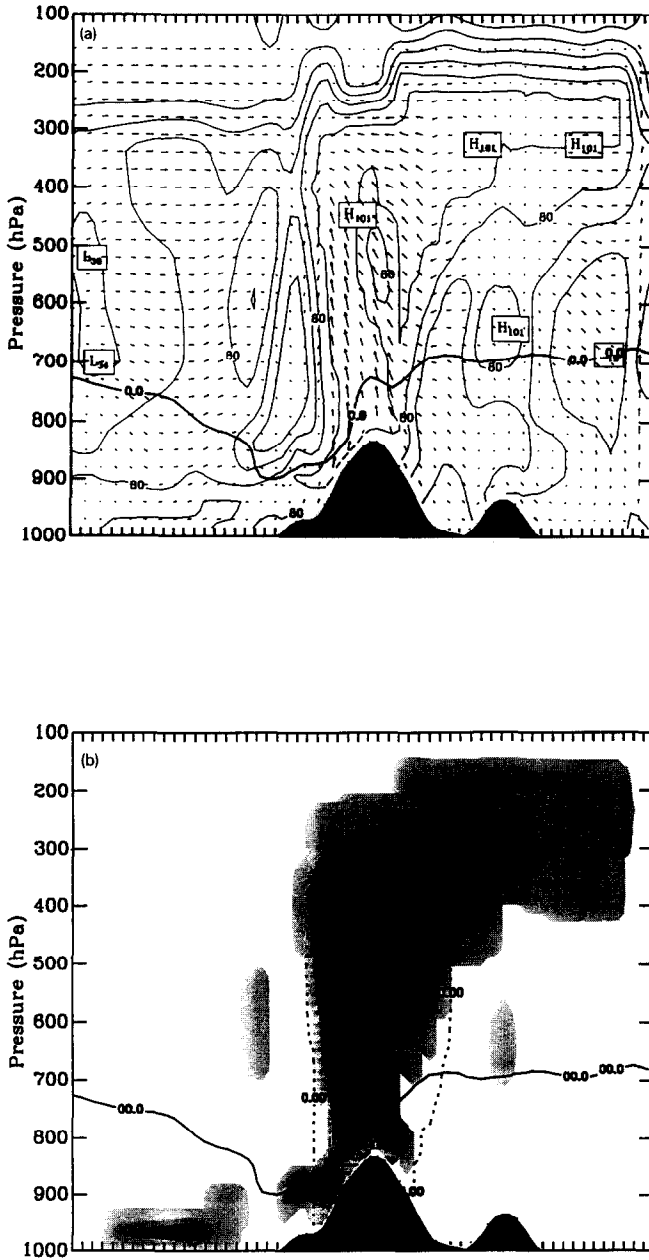


Fig. 7. As Fig. 6, but for the WARM simulation. Maximum wind speeds in the horizontal and vertical direction are  $25.75 \text{ m s}^{-1}$  and  $0.092 \text{ Pa s}^{-1}$ . Contour lines range from 0.001 to 1.4 g/kg by steps of 0.05 g/kg for rainwater. This option does not predict ice. Grey levels are at 0.001, 0.05, 0.1, 0.15, 0.2, 0.25, 0.3, 0.35 and 0.4, respectively.

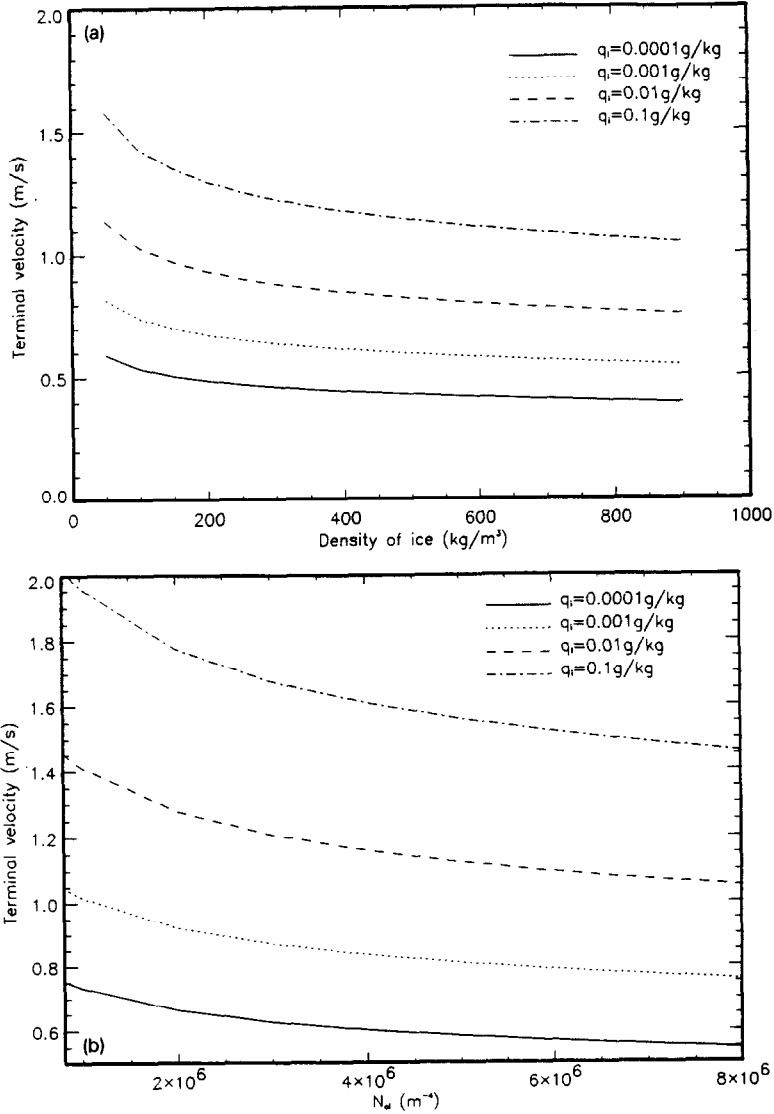
the interaction of dynamics and ice microphysical processes results in changes of the wind circulation due to falling rain and/or ice. In some regions, for example, downward motions develop below the 0°C isotherm due to cooling by melting of ice. In cloudy regions the WARM simulation calculates slightly higher temperature values than the COLD run, where the discrepancies result from the different amounts of the released latent heat or absorbed heat.

In the upper model layers higher values of relative humidity are predicted by the WARM simulation than by the COLD run (and all other ice-including simulations). This mirrors in larger vertical and horizontal extensions of the clouds (Figs. 6 and 7). The reason is that a lot of moisture is lifted into higher levels due to strong vertical motions at the French Riviera. Once formed in the upper levels, the cloud water is transported northeastwards. Since the cloud water mixing ratio is not beyond the threshold value used by the Kessler-type parameterization for the onset of rainwater formation, no rain is formed. Thus, evaporation, until saturation is reached, is the only sink for cloud water. Consequently, the upper model domain is moistened during the transport of cloud water. On contrary, clouds containing ice also lose water by sedimentation. Hence, the cloud tops are found in lower levels than those predicted by the WARM run (Figs. 6 and 7). Furthermore, in the COLD run condensate may be formed at lower relative humidity with respect to water (cf., Eqs. 6 and 7). Note that at some grid points only one of the simulations predicts clouds which results from the differences in the distributions of moisture caused by different dynamics and microphysical processes.

The WARM and COLD simulations, of course, predict similar distributions of cloud water mixing ratios when the temperature is above freezing. But below freezing large differences exist. Compared with the COLD run, the WARM simulation predicts higher amounts of cloud water for this region and the maxima of cloud water mixing ratios predicted occur in higher levels (Figs. 6 and 7). The reasons are manifold. In the COLD run the excess moisture is partitioned in condensation and water vapor deposition and ice crystals grow at the cost of cloud droplets. Furthermore, riming which competes with the rainwater formation via autoconversion and accretion, is an additional sink for cloud water. Consequently, at these temperatures (i.e., at these levels) the rainwater mixing ratios predicted by the COLD simulation are also lower than those predicted by the WARM simulation. In some clouds of the COLD run rainwater is formed via ice phase when ice particles falling through the level of freezing melt (e.g., over the Carpathians Figs. 6 and 7). In the WARM run, however, no rainwater occurs at this location because the cloud water present does not exceed the threshold value for the onset of rainwater formation.

The high amounts of ice topped clouds observed from satellite suggest that most of the rain was formed via ice phase during the simulated episode. Out of all simulations the precipitation fields predicted by the WARM simulation show less horizontal gradients and less horizontal extension. The inclusion of ice microphysics effects that in the COLD simulation precipitation begins earlier than in the WARM run, because only the presence of ice is decisive to initiate the sedimentation, i.e., no threshold value as required by the Kessler scheme must be exceeded. Further differences in the predicted precipitation fields result from the different terminal velocities of rainwater and ice (Fig. 8) which cause different fluxes of the total water. In contrast to the COLD run, the WARM simulation underestimates the 72 h accumulated rain rates. The BIAS score, threat score and categorical

score indicate that for low threshold amounts of precipitation the WARM simulation provides a better precipitation forecast than the COLD run (and the other simulations). On contrary, for higher threshold values of precipitation the COLD simulation leads to better results (Fig. 3). Over the Alps the 72 h accumulated rain rate is predicted up to 32.7 mm lower by the WARM simulation than by the COLD run because the important path of the precipitation formation processes via the ice phase is not included in the WARM run. Only at a few grid points the accumulated precipitation is less for the COLD run (up to 2 mm) than for the WARM simulation.



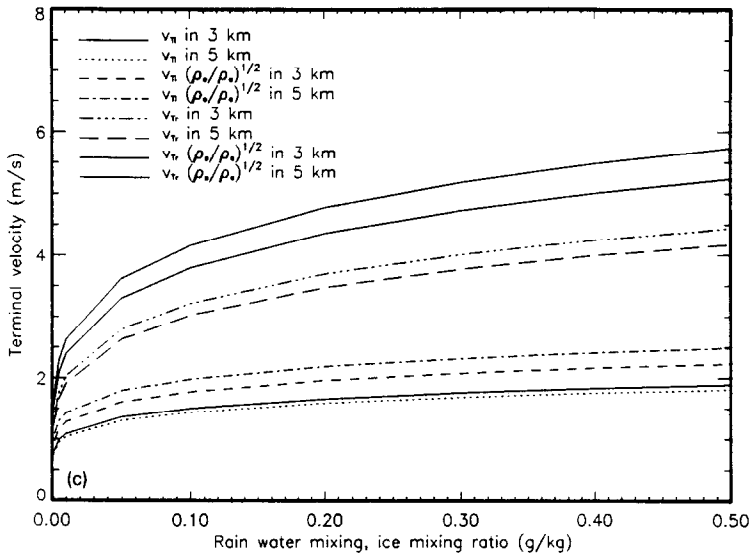


Fig. 8. Influence of (a) the density of ice, (b) the choice of  $N_{oi}$  both at an altitude of 6 km, and (c) of the correction term for air density variation on the massweighted terminal velocities for different rainwater and ice mixing ratios.

### 3.3. Simulation without riming (NOR)

Riming seems to be an important ice forming process (e.g., Cotton and Anthes, 1989). In order to study the significance of riming on cloud structure and precipitation formation on a regional scale, the MM4 with ice parameterization was also run without riming. As shown in Fig. 9, the predicted meteorological fields and the predicted distributions of clouds do not differ strongly from that of the COLD run (Fig. 6).

Since riming is a competitive process to autoconversion and accretion the largest differences occur in the regions of coexistence of ice and supercooled water. Here, less supercooled cloud and rainwater and larger ice mixing ratios are predicted by the COLD run, rather than by the NOR simulation. If no riming is considered, the threshold value for the onset of autoconversion is passed earlier and rainwater is formed earlier, too. But riming seems to be a major sink for cloud water only in the case of strong vertical motions and strong convection. This is the case at the French Riviera, and in some areas over the Atlantic ocean, Scandinavia and the Alps. The predicted relative humidity is higher for the NOR run than for the COLD simulation, but the maximum and minimum values of this quantity only differ slightly.

Surprisingly, the 72 h accumulated rain did not differ substantially from that of the COLD run when riming is not activated. With respect to the measures of skill for low threshold values of precipitation the NOR simulation usually provides a similar precipitation forecast as the COLD run; for high threshold values the latter leads to slightly better results than the former (Fig. 3). On the basis of an over-all evaluation, i.e., the calculated estimation skills (Threat score, BIAS-score and categorical score) and the comparison with the observed pattern as well as the temporal development of the precipitation, the inclusion of riming

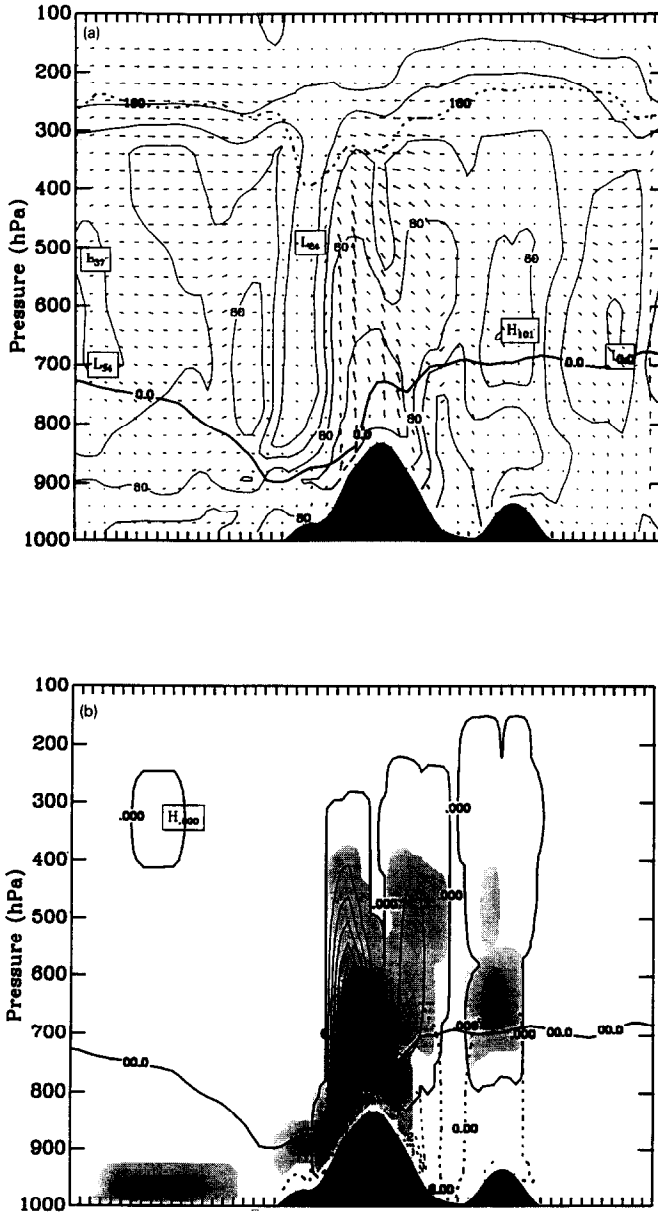


Fig. 9. As Fig. 6, but for the NOR simulation. Maximum wind speeds in the horizontal and vertical direction are  $26.42 \text{ m s}^{-1}$  and  $0.110 \text{ Pa s}^{-1}$ . Contour lines range from 0.001 to 2.25 g/kg by steps of 0.05 g/kg for rainwater and from 0.001 to 0.5 g/kg by steps of 0.05 g/kg for ice, respectively. Grey levels are at 0.001, 0.05, 0.1, 0.15, 0.2, 0.25, 0.3, 0.35, 0.4, respectively.

produces a better precipitation forecast. Note that typical annual values of correct categorical forecast range about 0.81 to 0.86 (Anthes, 1983). This may indicate that riming should also be included in regional weather forecast models.

#### 3.4. Studies on the sedimentation

In the calculation of the massweighted terminal velocity the density of ice is required. As already mentioned, the density of ice is highly variable. It can be derived from Eqs. (4) and (5) that the terminal velocity decreases with increasing density of ice (see also Fig. 8).

Two additional sensitivity studies were carried out using a density of ice of  $\rho_i = 600 \text{ kg m}^{-3}$  (as used by Cotton et al. (1982) for graupel) and of  $\rho_i = 916 \text{ kg m}^{-3}$  (solid ice; hail) denoted as COLD600 and COLD916, respectively. In the layers with temperatures lower than  $0^\circ\text{C}$ , the predicted ice mixing ratios are almost higher in the COLD600 and COLD916 studies than in the COLD simulation where the highest values are predicted by the COLD916 run. The opposite is found for the mixing ratios of rainwater and cloud water. In most of the cases, the predicted accumulated precipitation is higher for the COLD simulation than for the additional sensitivity studies. After 72 h of simulation, for instance, the accumulated precipitation over the Alps is up to 3 mm less for the COLD600 simulation and up to 9.2 mm less for the COLD916 simulation than for the COLD simulation.

Different values for  $N_{oi}$  are documented in the literature. If  $N_{oi}$  is altered by an order of magnitude the terminal velocity changes by about  $0.5 \text{ m s}^{-1}$  assuming an ice mixing ratio of  $0.1 \text{ g kg}^{-1}$  at an altitude of 6 km (Fig. 8).

As already mentioned, the correction term  $(\rho_o/\rho_a)^{1/2}$ , considering the effect of the air density variations on the calculated terminal velocity, is often neglected. Fig. 8 illustrates the effect of this term at different altitudes for varying rainwater and ice mixing ratios. The results of a sensitivity study using this density correction term (DECOR) indicate a large effect of the correction term on the cloud extensions, i.e., the clouds, especially the cloud tops of deep clouds consisting of ice, are found in lower model layers than those of the COLD run because the terminal velocity calculated with the correction term is higher in the upper levels. The effect may be artificially enhanced by the poor vertical resolution of 1 to 3 km in the upper part of the model which can pretend large differences in the cloud tops even if the cloud tops of both runs differ only a few dekameters when a better vertical resolution would be used. In the levels between 600 hPa and 300 hPa the relative humidities are slightly lower for the DECOR study than for the COLD run. The values of rainwater mixing ratio predicted by the DECOR study are often lower than for the COLD run. No significant rainwater mixing ratios, for instance, are found in the upper part of the clouds in the DECOR study. The lower values of mixing ratio of rainwater and ice in the latter study result from the enforced sedimentation in the upper troposphere. In the subsaturated regions below the clouds larger amounts of ice or rainwater can evaporate which results in slight temperature differences between both simulations. The 72 h accumulated precipitation distributions are similar for the DECOR and the COLD runs, but up to 7.5 mm higher values are predicted for the Mediterranean area and up to 1.6 mm lower values for the Atlantic region by the DECOR run.

### 3.5. Cloud droplet spectra

Obviously, the cloud droplet spectra vary from cloud to cloud and from cloud type to cloud type (e.g., Cotton and Anthes, 1989). Berry (1968) formulated an autoconversion rate which allows to take into account the properties of the environment of the cloud. This autoconversion rate depends on the initial cloud droplet concentration as well as on the dispersion of the cloud droplet distribution. In order to investigate the influence due to the parameterizations of the autoconversion and the cloud droplet spectra, two sensitivity studies, one for a continental and one for a maritime aerosol spectrum, were performed using the warm scheme (to avoid effects and changes resulting from ice processes). The results of these studies are compared with those of the WARM simulation which uses a Kessler-type autoconversion. In contrast to the Kessler parameterization, where rainwater is only formed if the cloud water mixing ratio is beyond a certain threshold value, the formulation of Berry allows the rainwater formation also for very low cloud water mixing ratios. From the theoretical point of view the differences between the autoconversion rates increase with increasing cloud water mixing ratios (Doms and Herbert, 1985). The numerical simulations, however, show no significant effects due to the different parameterizations of autoconversion on the predicted cloud distributions and on the behavior of the simulated clouds. This is in substantial agreement with Doms and Herbert (1985). Small differences especially occur in the local and temporal cloud formation. Sometimes, rain reaches the ground earlier when the Berry-type parameterization is used. Like the WARM run, the simulations using the Berry-type autoconversion produces similar unrealistic results of too high relative humidity and cloud water over the anticyclone over Russia. This phenomenon indicates that in the upper model atmosphere the rainwater formation by warm path processes alone is not efficient enough to remove the moisture.

## 4. Conclusions

An ice parameterization scheme has been developed and tested in a mesoscale  $\alpha$  weather forecast model. Liquid water is assumed to consist of cloud water and rainwater. The important processes to be used in the parameterization scheme are condensation and deposition of water vapor, formation of rainwater by autoconversion, accretion and melting, evaporation of both cloud and rainwater, sublimation, as well as riming of supercooled cloud water onto ice crystals. The ice phase particles considered are ice crystals which are not highly rimed. They are initiated from activated ice nuclei which are assumed to occur in a sufficient number. The ice parameterization scheme has been exercised in a weather situation, when heavy rainfall occurred over Europe. The experiments demonstrated that the ice parameterization is able to simulate qualitatively the evolution of cloudiness and precipitation.

Different values for the density of ice, the terminal velocity and the temperature limit for the existence of supercooled water droplets are considered. Furthermore, two different parameterization schemes for warm cloud processes, the Kessler and the Berry scheme, respectively, and the ice parameterization with and without riming can be activated. Several experiments have been performed in order to investigate the sensitivity of the model to

different parameters and processes. It is substantiated by all of these numerical experiments that the relative humidity and water substance mixing ratio fields were strongly altered by turning off the ice phase or the riming process.

Many features simulated by the model using the ice parameterization scheme were in acceptable agreement with observations, in particular, the fields of relative humidity and precipitation. It was illustrated that the incorporation of the ice parameterization gives a more realistic description of the dynamics and microphysics of the troposphere. The ice parameterization was found to be an improvement of the warm scheme. The major deficiencies of the latter occur when strong upward vertical transport of humidity are present or when the clouds are strongly glaciated (Mölders et al., 1994). This is true for both the Kessler- and the Berry-type autoconversion. In contrast to the Kuo-type cumulus parameterization scheme which can be used alternatively in MM4 (Anthes et al., 1987; Mölders et al., 1994), the ice parameterization as well as the warm scheme are also valid for finer mesh sizes of the computational grid.

### Acknowledgements

We are grateful to M.P. Scheele and G.H.L. Verver from the KNMI (Koninklijk Nederlands Meteorologisch Instituut) who gave access to the precipitation data. We gratefully acknowledge the support from H.J. Jakobs from the EURAD group (Rheinisches Institut für Umweltforschung at Cologne) who friendly helped in questions with the processing of MM4 and the MM4 data. He also gave access to the MM4 graphic routines. We should express our thanks to the anonymous reviewers for fruitful discussions, helpful comments and critical questions. Computational support came from the Research Center Jülich (KFA), in particular from ZAM, HLRZ, ICH2 and ICH3. This work was funded by the Ministry of Research and Technology (BMFT) of Germany and the Ministry for Science and Research (MWF) of the State Nordrhein-Westfalen.

### References

- Anthes, R.A., 1977. A cumulus parameterization scheme utilizing a one-dimensional cloud model. *Mon. Weather Rev.*, 107: 963–984.
- Anthes, R.A., 1983. Review: Regional models of the atmosphere in middle latitudes. *Mon. Weather Rev.*, 111: 1306–1335.
- Anthes, R.A. and Warner, T.T., 1978. Development of hydrodynamic models suitable for air pollution and other mesometeorological studies. *Mon. Weather Rev.*, 106: 1045–1078.
- Anthes, R.A., Hsie, E.-Y. and Kuo, Y.-H., 1987. Description of the Penn State/NCAR Mesoscale Model Version 4 (MM4), NCAR/TN-282+STR.
- Anthes, R.A., Kuo, Y.-H., Hsie, E.-Y., Low-Nam, S. and Bettge, T.W., 1989. Estimation of skill and uncertainty in regional numerical models. *Q. J. R. Meteorol. Soc.*, 115: 763–806.
- Beard, K.V., 1977. Terminal velocity adjustment for cloud and precipitation drops aloft. *J. Atmos. Sci.*, 34: 1293–1298.
- Berry, E.X., 1968. Modification of the warm rain process. Preprints 1st Natl. Conf. Weather Modification. Albany, pp. 81–88.
- Cotton, W.R. and Anthes, R.A., 1989. *Storms and Cloud Dynamics*. Academic Press Inc., San Diego.

- Cotton, W.R., Stephens, M.A., Neuhorn, T. and Tripoli, G.J., 1982. The Colorado State University Three-Dimensional Cloud Mesoscale Model 1982. Part II: An Ice Phase Parameterization. *J. Rech. Atmos.*, 16: 295–320.
- Cotton, W.R., Tripoli, G.J., Rauber, R.M. and Mulvihill, E.A., 1986. Numerical simulations of the effects of varying ice crystal nucleation rates and aggregation processes on orographic snowfall. *J. Clim. Appl. Meteorol.*, 25: 1658–1680.
- Doms, G. and Herbert, F., 1985. Fluid- und Mikrodynamik in numerischen Modellen konvektiver Wolken. *Ber. Inst. Meteorol. Geophys., Univ. Frankfurt/Main*, 62 (in German).
- Dudhia, J., 1989. Numerical study of convection observed during the winter monsoon experiment using a mesoscale two-dimensional model. *J. Atmos. Sci.*, 46: 3077–3106.
- Fletcher, N.H., 1962. *The Physics of Rain Clouds*. Cambridge University Press.
- Heymsfield, A., 1977. Precipitation development in stratiform ice clouds: A microphysical and dynamical study. *J. Atmos. Sci.*, 34: 367–381.
- Heymsfield, A.J. and Sabin, R.M., 1989. Cirrus crystal nucleation by homogeneous freezing of solution droplets. *J. Atmos. Sci.*, 46: 2252–2264.
- Hobbs, P.V., Radke, L.F., Fraser, A.B., Locatelli, J.D., Robertson, D.G., Atkinson, R., Farber, J., Weiss, R.R. and Easter, R.C., 1972. Field Observations and Theoretical Studies of Clouds and Precipitation over the Cascade Mountains and their Modification by Artificial Seeding (1971–1972). *Res. Rep. VII, Dep. Atmos. Sci. Univ. Washington, Seattle*, 293 pp.
- Hsie, E.-Y. and Anthes, R.A., 1984. Simulations of frontogenesis in a moist atmosphere using alternative parameterizations of condensation and precipitation. *J. Atmos. Sci.*, 41: 2701–2716.
- Huffman, P.J., 1973. Supersaturation spectra of AgI and natural ice nuclei. *J. Appl. Meteorol.*, 12: 1080–1082.
- Kessler, E., III, 1969. On the Distribution and Continuity of Water Substance in Atmospheric Circulations. *Meteorol. Monogr.*, 27. *Am. Meteorol. Soc.*, 84 pp.
- Koenig, L.R. and Murray, F.W., 1976. Ice-bearing cumulus cloud evolution: Numerical simulations and general comparison against observations. *J. Appl. Meteorol.*, 15: 747–762.
- Kuo, H.L., 1974. Further studies of the parameterization of the influence of cumulus convection on large-scale flow. *J. Atmos. Sci.*, 31: 1232–1240.
- Laube, M. and Höller, H., 1988. Cloud physics. In *Landolt-Börnstein, Gruppe V: Geophysik und Weltraumforschung*, pp. 1–100.
- Leary, C.A. and Houze, R.A., Jr., 1979. Melting and evaporation of hydrometeors in precipitation from the anvil clouds of deep tropical convection. *J. Atmos. Sci.*, 36: 669–679.
- Lin, Y.-L., Farley, R.D. and Orville, H.D., 1983. Bulk parameterization of the snow field in a cloud model. *J. Clim. Appl. Meteorol.*, 22: 1065–1092.
- Lui, J.Y. and Orville, H.D., 1969. Numerical modeling of precipitation and cloud shadow effects on mountain-induced cumuli. *J. Atmos. Sci.*, 26: 1283–1298.
- Locatelli, J.D. and Hobbs, P., 1974. Fall speeds and masses of solid precipitation particles. *J. Geophys. Res.*, 79: 2185–2197.
- Lord, S.J., Willoughby, H.E. and Piotrowicz, J.M., 1984. Role of a parameterized ice-phase microphysics in an axisymmetric, nonhydrostatic tropical cyclone model. *J. Atmos. Sci.*, 41: 2836–2848.
- Marshall, J.S. and Palmer, W.M., 1948. The distribution of raindrops with size. *J. Meteorol.*, 5: 165–166.
- Meyers, M.P., DeMott, P.J. and Cotton, W.R., 1992. New primary ice-nucleation parameterizations in an explicit cloud model. *J. Appl. Meteorol.*, 31: 708–721.
- Mölders, N., 1993. *Wolkenparametrisierung für ein Chemie-Transportmodell*. *Mitt. Inst. Geophys. Meteorol., Univ. Köln*, 88, Ph. D. Thesis (in German).
- Mölders, N., Hass, H., Jakobs, H.J., Laube, M. and Ebel, A., 1994. Some effects of different cloud parameterizations in a mesoscale model and a chemistry transport model. *J. Appl. Meteorol.*, 33: 527–545.
- Mölders, N. and Laube, M., 1994. A numerical study on the influence of different cloud treatment in a chemical transport model on gasphase distribution. *Atmos. Res.*, 32: 249–272.
- Orville, H.D. and Kopp, F.J., 1977. Numerical simulation of the life history of a hailstorm. *J. Atmos. Sci.*, 34: 1596–1618.
- Phillips, P.D., Richner, H., Joss, J. and Ohmura, A., 1981. ASOND-78: An intercomparison of Väisälä, VIZ and Swiss Radiosondes. *Pageoph.*, 119: 259–277.
- Pruppacher, H.R. and Klett, J.D., 1980. *Microphysics of Clouds and Precipitation*. Reidel, Dordrecht, 741 pp.

- Scheele, M.P. and Verver, G.H.L., 1990. Objective analysis of precipitation observations during the Chernobyl episode. Technical report, TR-122, Koninklijk Nederlands Meteorologisch Instituut, De Bilt.
- Srivastava, R.C., 1967. A study of effects of precipitation on cumulus dynamics. *J. Atmos. Sci.*, 24: 36–45.
- Tripoli, G.J. and Cotton, W.R., 1980. A numerical investigation of several factors contributing to the observed variable intensity of deep convection over south Florida. *J. Appl. Meteorol.*, 19: 1037–1063.
- Willis, P. and Heymsfield, A.J., 1989. Structure of the melting layer in mesoscale convective system stratiform precipitation. *J. Atmos. Sci.*, 46: 2008–2025.
- Zhang, D.-L., 1989. The effect of parameterized ice microphysics on the simulation of vortex circulation with mesoscale hydrostatic model. *Tellus*, 41A: 132–147.
- Zikmunda, J. and Vali, B., 1972. Fall patterns and fall velocities of rimed ice crystals. *J. Atmos. Sci.*, 29: 1334–1347.